

SUPPLEMENTARY INFORMATION for Biexciton and Trion Energy Transfer from CdSe/CdS Giant Nanocrystals to Si Substrates

Tianle Guo,[†] Siddharth Sampat,[†] Sara M. Rupich,[‡] Jennifer A. Hollingsworth,[¶]
Matthew Buck,[¶] Han Htoon,[¶] Yves J. Chabal,[‡] Yuri N. Gartstein,[†] and Anton
V. Malko^{*,†}

*Department of Physics, The University of Texas at Dallas, Richardson, TX, 75080, USA,
Department of Material Science, The University of Texas at Dallas, Richardson, TX,
75080, USA, and Materials Physics & Applications: Center for Integrated
Nanotechnologies, Los Alamos National Laboratory, Los Alamos, New Mexico, 87545, USA*

E-mail: anton.malko@utdallas.edu

*To whom correspondence should be addressed

[†]Department of Physics, The University of Texas at Dallas, Richardson, TX, 75080, USA

[‡]Department of Material Science, The University of Texas at Dallas, Richardson, TX, 75080, USA

[¶]Materials Physics & Applications: Center for Integrated Nanotechnologies, Los Alamos National Laboratory, Los Alamos, New Mexico, 87545, USA

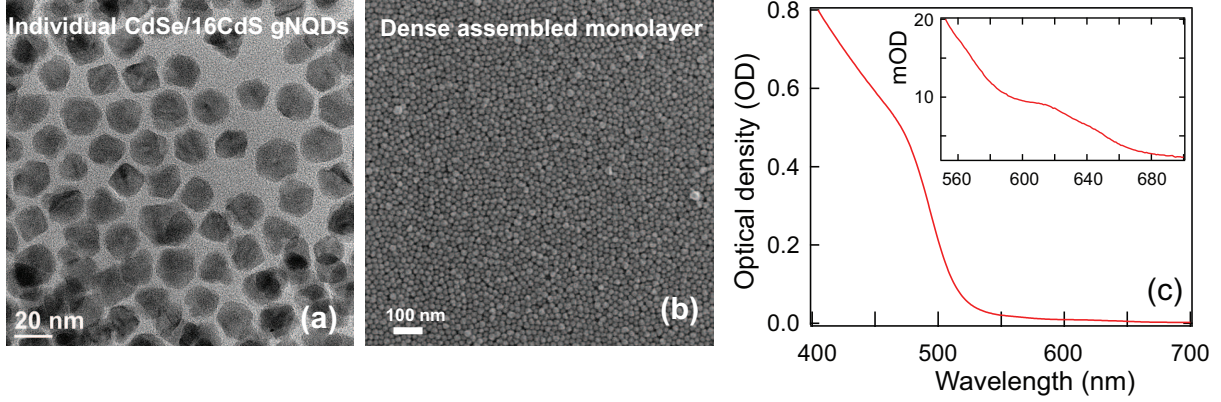


Figure S1: (a)TEM images of individual CdSe/16CdS gNQDs; (b)SEM of a dense monolayer of gNQDs assembled on Si; (c) Optical absorption spectra of a gNQD solution. Inset: expanded view showing lowest energy excitonic transitions of the CdSe core.

Comments for Figure S1

The TEM images of individual gNQDs show average diameter of $\sim 18 - 20$ nm, corresponding well to the starting diameter of CdSe core ~ 5 nm followed by the deposition of 16 CdS shells (monolayer CdS thickness of ~ 0.375 nm) *via* SILAR. SEM of a monolayer of gNQDs assembled on pre-functionalized Si surface. Very uniform coverage is attained. Optical absorption spectra of a solution of gNQDs in hexane. As expected, absorption in CdS shell dominates starting ~ 520 nm, due to much larger volume of the shell material as compared to the CdSe core.

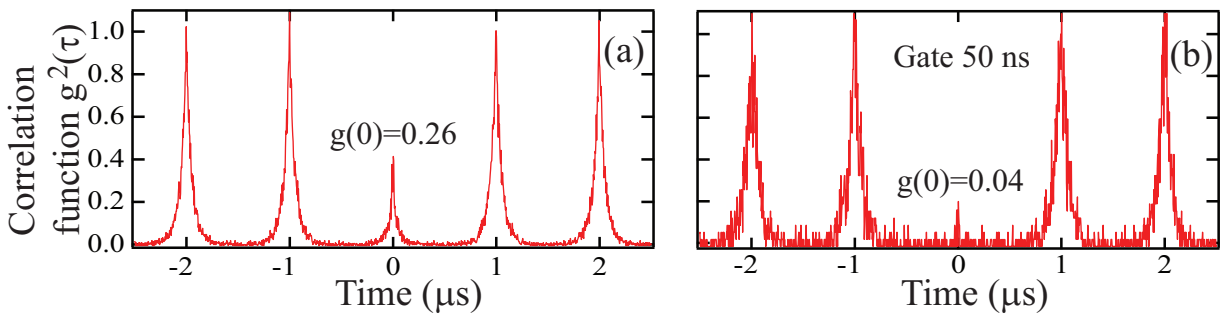


Figure S2: (a) Second order correlation function $g^2(\tau)$ for the single gNQD shown in main Figure 1. (b) Recomputed $g^2(\tau)$ function, with applied 50 ns gate

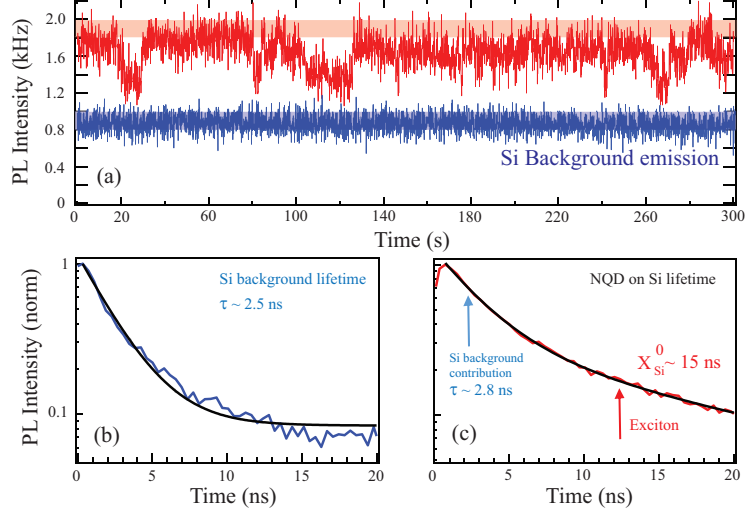


Figure S3: (a) Blinking trace for single gNQD on Si; (b) PL lifetime of the Si only background, from the blue-shaded region in panel (a); (c) NQD PL lifetime from the red-shaded emission intensity level in panel (a).

Comments for Figure S3

As discussed in the main text, measurements of the PL intensities and lifetimes for individual NQDs deposited on Si substrates provides a potential opportunity to directly measure transfer rates for different excitonic species that are observable in the PL intensity trace. However, large optical power required to excite single NQD also generates large background emission from the Si substrate. This emission background represents nearly half of the total PL intensity and has fast, $\sim 1 - 4$ ns, lifetime masking the appearance of the multiexciton species.

Section 1: Detailed analysis of the PL intensity levels and lifetimes from single NQD data

We analyze PL intensity levels and decay traces extracted from the color coded areas as shown in Figure 1 of the manuscript main text. A certain PL intensity level I_i can be ascribed to each of the states and the experimentally measured PL quantum yield (QY^i) is given by the ratio of the intensity of the state to the intensity of X^0 : $QY^i = I_i/I_{X^0}$ assuming

that $QY(X^0)=1$.¹ Using average PL intensities from the shaded regions in Figure 1 for each of the emissive states, we find $QY(X^-)=0.54$ and $QY(X^+)=0.43$. High values of the X^\pm quantum yields imply that for these species, Auger rates are comparable to radiative decay rates. Exponential fits to PL decays in Figure 1 (b) in the main text yield the lifetimes $\tau_{\text{rad}}^0 = 47\text{ns}$, $\tau^{X^-} = 15\text{ns}$ and $\tau^{X^+} = 12\text{ns}$. The radiative decay rate γ_{rad}^i of a charged state “ i ” can be related to the decay rate of the neutral exciton, γ_{rad}^0 as in equation 1,

$$\gamma_{\text{rad}}^i = \beta^i \gamma_{\text{rad}}^0. \quad (1)$$

while the quantum yield of a charged state “ i ” in the presence of a non-radiative Auger process is defined as shown in equation 2

$$QY^i = \frac{\gamma_{\text{rad}}^i}{\gamma_{\text{rad}}^i + \gamma_A^i} \quad (2)$$

where γ_A^i is Auger decay rate of this state.

As the result, following expressions relate Auger rates of the trions, experimentally measured quantum yields, QY^{X^\pm} , measured PL lifetimes, τ^{X^\pm} and β factors.

$$\beta^{X^\pm} = \frac{QY^{X^\pm} \tau_{\text{rad}}^0}{\tau^{X^\pm}} \quad (3a)$$

$$\gamma_A^{X^\pm} = \gamma_{\text{rad}}^{X^\pm} \left(\frac{1}{QY^{X^\pm}} - 1 \right) \quad (3b)$$

$$\frac{1}{\tau^{X^\pm}} = \gamma^{X^\pm} = \gamma_{\text{rad}}^{X^\pm} + \gamma_A^{X^\pm} \quad (3c)$$

Using the measured values of quantum yields and lifetimes of X^\pm and X^0 , we extract $\beta^{X^-} \sim 1.7$ and $\beta^{X^+} \sim 1.7$, in close agreement with previous measurements.^{2,3} The values of β differ from the ideal case of $\beta_{\text{stat}} = 2$ due to mutual repulsion of the like charges reducing wavefunction overlap in a shallower-confined CdSe/CdS gNQDs.^{2,3} The extracted

trion Auger decay rates, $\gamma_A^{X^\pm}$ range from 0.031 ns^{-1} for X^- to 0.048 ns^{-1} for X^+ , clearly comparable to radiative decay rate of the exciton, $\gamma_{\text{rad}}^0 = 0.021 \text{ ns}^{-1}$

Similarly, previous work have shown that Auger rates and PL lifetime for neutral biexciton species can be written as:

$$\gamma_A^{BX} = 2(\gamma_A^{X^-} + \gamma_A^{X^+}) \quad (4a)$$

$$\frac{1}{\tau^{BX}} = \gamma^{BX} = \gamma_{\text{rad}}^{BX} + \gamma_A^{BX} \quad (4b)$$

In case of a neutral biexciton, statistical $\beta = 4$, however, taking into account electron delocalization, more representative figure is estimated as $\beta^{BX} \approx (\beta^{X^-} + \beta^{X^+}) \sim 3.4$. Using equations 1, 3b and 4b we compute Auger rate and expected emission lifetime for biexcitons as $\gamma_A^{BX} = 0.16 \text{ ns}^{-1}$ and $\tau^{BX} \sim 4.3 \text{ ns}$, closely matching BX lifetime extracted from correlation data and shown in main Figure 1(c). Similarly, using equation 2, we estimate $QY^{BX} \sim 0.3$, close to the value shown by $g^2(0)$ in Fig. S2 of this Supplementary Info.

Section 2: Calculation of transfer efficiencies for trions and biexcitons

Here we compute ET efficiencies for trions and biexcitons. As per Eq. 1 in the main text, ET efficiency of the multiexciton species " i " (" i " either trion or biexciton) is given by:

$$\eta^i = \gamma_{\text{RET}}^i / \gamma_{\text{Si}}^i; \quad \gamma_{\text{Si}}^i = \gamma_{\text{al}}^i + \gamma_{\text{RET}}^i + \gamma_A^i. \quad (5)$$

where we took into account that $\gamma_{\text{NRET}}^i \simeq 0$ for distances on the order of 10 nm. Further, as per Eq. 3 of the main text, the total decay rate of the species " i " on glass substrate relates

to the decay rate of the neutral exciton on the same substrate as:

$$\gamma_{\text{SiO}_2}^i = \gamma_{\text{A}}^i + \beta^i \gamma_{\text{rad, SiO}_2}^0 \quad (6)$$

Analogously to expressions shown in the main text for neutral exciton, the emission rate of the “allowed” light from species “ i ”, γ_{al}^i and their radiative decay rate on glass, $\gamma_{\text{rad, SiO}_2}^i$ are related to their spontaneous decay rate in vacuum γ_{vac}^i as:

$$\gamma_{\text{al}} \simeq 0.6\gamma_{\text{vac}}^i; \quad \gamma_{\text{rad, SiO}_2}^i = \beta^i \gamma_{\text{rad, SiO}_2}^0 \simeq 1.6\gamma_{\text{vac}}^i.$$

These relations are easily understood as modifications to radiative decay rate of the emitter in the vicinity of the substrate with higher density of the photonic modes to couple to.

Finally, we re-write RET rate to Si in terms of radiative emission rate of neutral exciton on glass, $\gamma_{\text{rad, SiO}_2}^0$, and observed total decay rates of species “ i ” on Si, γ_{Si}^i and on glass, $\gamma_{\text{SiO}_2}^i$:

$$\gamma_{\text{RET}}^i = \gamma_{\text{Si}}^i - \gamma_{\text{SiO}_2}^i + \beta^i \gamma_{\text{rad, SiO}_2}^0 \left(1 - \frac{0.6}{1.6}\right);$$

thus arriving at the expression for the transfer efficiency:

$$\eta^i = 1 - \frac{1}{\kappa_{\text{obs}}^i} + \beta^i \left(1 - \frac{0.6}{1.6}\right) \frac{\gamma_{\text{rad, SiO}_2}^0}{\gamma_{\text{Si}}^i} \quad (7)$$

where κ_{obs}^i stands for familiar ratio of total measured decay rates of species “ i ” on Si and glass, $\kappa_{\text{obs}}^i = \frac{\gamma_{\text{Si}}^i}{\gamma_{\text{SiO}_2}^i}$. Considering ET of neutral excitons (X^0) for which $\beta^0 = 1$, Eq. (7) translates to the familiar expression found in the main text:

$$\eta^0 = 1 - 0.6/1.6\kappa_{\text{obs}}^0 \quad (8)$$

Applying Eq. (7) to the average trion decay rates shown in Fig. 3 of the main text, we obtain $\eta^{\text{T}} \simeq 0.5$, where we utilized $\beta^{\text{T}} \simeq 1.7$. Similarly, using data from Fig. 4, we estimate $\eta^{\text{BX}} \simeq 0.45$ for $\beta^{\text{BX}} \simeq 3.4$. As can be invoked from the last term in Eq. (7), progressive acceleration of the radiative decay rate (bigger values of β) partially negates larger Auger

rates of BX species, leading to comparatively high values of η^{BX} .

Similarly, we can estimate bounds of BX efficiency from the linear fits of BX rates in Figure 5 of the main text. Using lower bound value of $\beta^{\text{BX}}=4.4$ and average fitted value of $\beta^{\text{BX}}=7$, we find $\eta^{\text{BX}} \sim 0.55 - 0.6$. While somewhat larger than what is found using $\beta = 3.4$ from single dot data, it still falls within bounds associated with large variability of the BX decay rates. Similarly, using two other data points for trion decays (the right-most squares on the trion decay line) as well as upper boundary for $\beta^{\text{T}} = 2.6$, we estimate maximum trion efficiency as $\eta^{\text{T}} \sim 0.65$. The variability in trion efficiency values is understandably smaller than those of BXs due to much smaller variance of the Auger rates.

Section 3: Effective relationship between decay rates in inhomogeneous samples

Here we illustrate the possible origin of the substrate-dependent effective relationship

$$\gamma^i = a^i + b^i \gamma^0. \quad (9)$$

between the experimentally measured decay rate γ^i of higher-order excited species i and the decay rate γ^0 of the neutral exciton. As discussed in the main text, the effect of the substrate in our case is to modify the radiative decay of the exciton: from its value of $\gamma_{\text{rad, SiO}_2}^0$ on the SiO₂ substrate it is accelerated to the value of $\gamma_{\text{rad, Si}}^0$ on Si:

$$\gamma_{\text{rad, Si}}^0 = \kappa_{\text{rad}} \gamma_{\text{rad, SiO}_2}^0. \quad (10)$$

The magnitude of the acceleration factor κ_{rad} depends on the distance from the NQD center to the substrate and has been evaluated to be around 2 – 2.5.

The form (9) assumes a linearized description within a small range of variability. Let variable x quantify the variations of the exciton radiative decay on the SiO₂ substrate around

$\bar{\gamma}$ value due to some inhomogeneity factor:

$$\gamma_{\text{rad,SiO}_2}^0 = \bar{\gamma} + x. \quad (11)$$

With the inclusion of a nonradiative exciton decay channel (rate γ_{nr}^0), the overall exciton decay rate $\gamma_{\text{SiO}_2}^0 = \gamma_{\text{nr}}^0 + \gamma_{\text{rad,SiO}_2}^0$ on SiO₂ substrate then reads as

$$\gamma_{\text{SiO}_2}^0 = \gamma_{\text{nr}}^0 + \bar{\gamma} + x. \quad (12)$$

As we discussed before, the radiative decay of higher-order excited species i is related to the exciton radiative decay by the beta-factor irrespectively of the substrate:

$$\gamma_{\text{rad,SiO}_2}^i = \beta^i \gamma_{\text{rad,SiO}_2}^0, \quad \gamma_{\text{rad,Si}}^i = \beta^i \gamma_{\text{rad,Si}}^0. \quad (13)$$

The Auger recombination γ_{A}^i is a very important decay channel for higher-order species, whose variability around γ_{nr}^i value due to the same inhomogeneity factor can be enhanced with respect to the dependence in Eq. (11):

$$\gamma_{\text{A}}^i = \gamma_{\text{nr}}^i + \alpha^i x, \quad (14)$$

α^i being the enhancement coefficient. With equations (12), (13) and (14) in place, the overall decay rate of the species i on the SiO₂ substrate $\gamma_{\text{SiO}_2}^i = \gamma_{\text{A}}^i + \gamma_{\text{rad,SiO}_2}^i$ becomes

$$\gamma_{\text{SiO}_2}^i = \gamma_{\text{nr}}^i - \alpha^i \bar{\gamma} - (\beta^i + \alpha^i) \gamma_{\text{nr}}^0 + (\beta^i + \alpha^i) \gamma_{\text{SiO}_2}^0. \quad (15)$$

Importantly, Eq. (15) is written down in the form of the effective Eq. (9) relating experimentally measured rates $\gamma_{\text{SiO}_2}^i$ and $\gamma_{\text{SiO}_2}^0$.

The analogous relationship between the measurable rates γ_{Si}^i and γ_{Si}^0 on the Si substrate is now derived in the same way with the modified radiative decay rates as per Eqs. (10) and

(13):

$$\gamma_{\text{Si}}^i = \gamma_{\text{nr}}^i - \alpha^i \bar{\gamma} - (\beta^i + \alpha^i / \kappa_{\text{rad}}) \gamma_{\text{nr}}^0 + (\beta^i + \alpha^i / \kappa_{\text{rad}}) \gamma_{\text{Si}}^0. \quad (16)$$

Once again, relationship (16) has the form of the effective Eq. (9) but with the coefficients a^i and b^i having generally changed with respect to those in Eq. (15). Comparing Eqs. (15) and (16), it is clear that upon transition to the Si substrate, the magnitude of the slope coefficient b^i is expected to decrease, while the magnitude of the offset coefficient a^i to increase. This is consistent with the type of behavior in experimental data shown in the main text.

Section 4: Table of Auger rates, scaling factors and ET efficiencies

Species	Measurement	Scaling	Auger Rates	Auger Rates	ET
Type	Type	Factors	on SiO ₂ , ns ⁻¹	on Si, ns ⁻¹	Efficiency
X^0		1	—	—	75 %
X^T	single dot	1.7 – 2	0.03 – 0.05	0.03	
	ensemble	~ 2.6	~ 0.03	~ 0.03	50 – 60 %
BX	single dot	3.4-4	0.16	—	
	ensemble	~ 4.4 – 7	~ 0.2	0.15 – 0.25	30 – 60 %

Comments:

The scaling factors and Auger rates for trions and biexcitons have been measured using single dot and ensemble measurements. Single dot data and details of calculations are shown in Section 1 of this Supplementary Info. Ensemble data are based on the Figure 5 of the main text. As discussed in the main text, Eq. (3), the y -axis intercept on Figure 5 will correspond to the Auger decay rate for the given species on a given substrate, while the tangent of the line would correspond to the scaling factor, β . All points for given species (either trions or biexcitons) match fairly well to a line fit. For trions (open squares on Figure 5), it is even possible to judge that points for “glassy” surfaces (blue and green squares)

fall along the same line as those corresponding to Si surfaces (red squares), with similar Auger rates $\gamma_A^T \sim 0.03 \text{ ns}^{-1}$ and $\beta \sim 2.6$. For biexcitons, there is much less accuracy in determination of the fit parameters as discussed in the main text and the Supplementary Info, Section 3 (large inhomogeneity of the Auger rates, effects of multiexponential fitting and “hidden” variable α^i). The fitting provides for $\gamma_A^{BX} \sim 0.15 - 0.3$ for “glassy” and Si surfaces, generally supporting our conclusion of Auger rates been largely unaffected by the nature of the interacting surface.

References

1. Park, Y.-S.; Malko, A. V.; Vela, J.; Ghosh, Y.; Garcia-Santamaria, F.; Hollingsworth, J. A.; Klimov, V. I.; Htoon, H. Near-Unity Quantum Yields of Biexciton Emission from CdSe/CdS Nanocrystals Measured Using Single-Particle Spectroscopy. *Phys. Rev. Lett.* **2011**, *106*, 187401.
2. Park, Y.-S.; Bae, W. K.; Pietryga, J. M.; Klimov, V. I. Auger Recombination of Biexcitons and Negative and Positive Trions in Individual Quantum Dots. *ACS Nano* **2014**, *8*, 7288–7296.
3. Sampat, S.; Karan, N. S.; Guo, T.; Htoon, H.; Hollingsworth, J. A.; Malko, A. V. Multistate Blinking and Scaling of the Recombination Rates in Individual Silica-Coated CdSe/CdS Nanocrystals. *ACS Photon.* **2015**, *2*, 1505–1512.